Chapter 4 Results and Discussion

In this chapter, we present experimental results of V shaped defects inverted pyramid on GaN film. AFM images of V-defects, the μ-Raman spectra of V-defects of different doping concentrations and different sizes are analyzed. They illustrate the carrier gathering inside V-defects caused by high dislocation density. LO phonon-plasmon coupling model and effective electron density were used to show the carrier concentration and dislocation density inside V-defects.

4-1 Morphology of V-defect

Optical and AFM images of samples A, B, and C are shown in Fig.4-1-1. The hexagonal pits with six triangular facets are called V-defect since they form the V-shape in cross section view, as shown in Fig.4-1-2(a). It is suggested that the hexagonal defect has the shape of inversion pyramid, formed by six symmetrical {10-11} facets or {11-22} facets[5,11] , as shown in Fig.4-1-2(b).

3D AFM images of different size V-defects on sample C are shown in Fig.4-1-3. Six evident side lines that divide the triangular facets can be observed in small V-defects (<4.8μm). The six side lines separate gradually into twelve and form additional six facets in larger V-defects. As the V-defect becomes larger, it becomes a polygon and circle-like finally. From the cross section profile of V-defect, the vertex angle can be determined by subtracting the left and right angles that between plain and facets. Vertex angles of different size V-defects are calculated and listed in Table4-1-1.

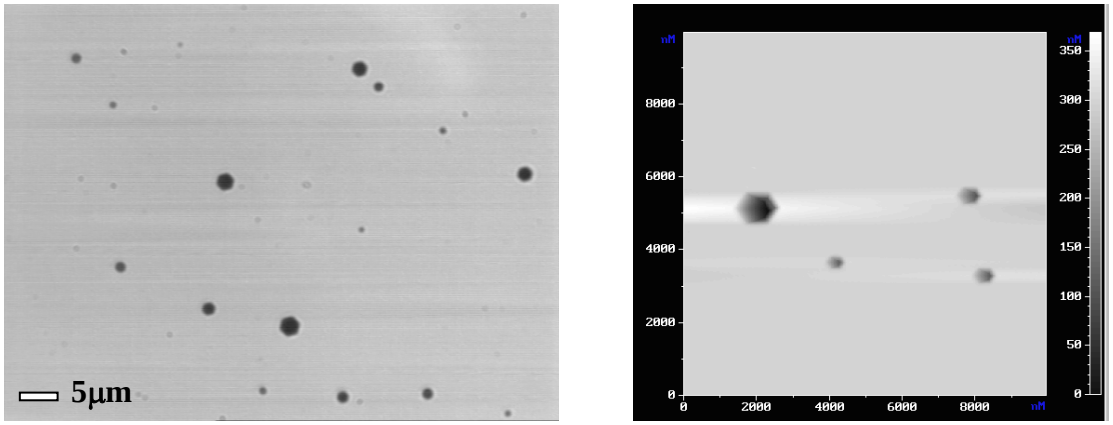

Sample A

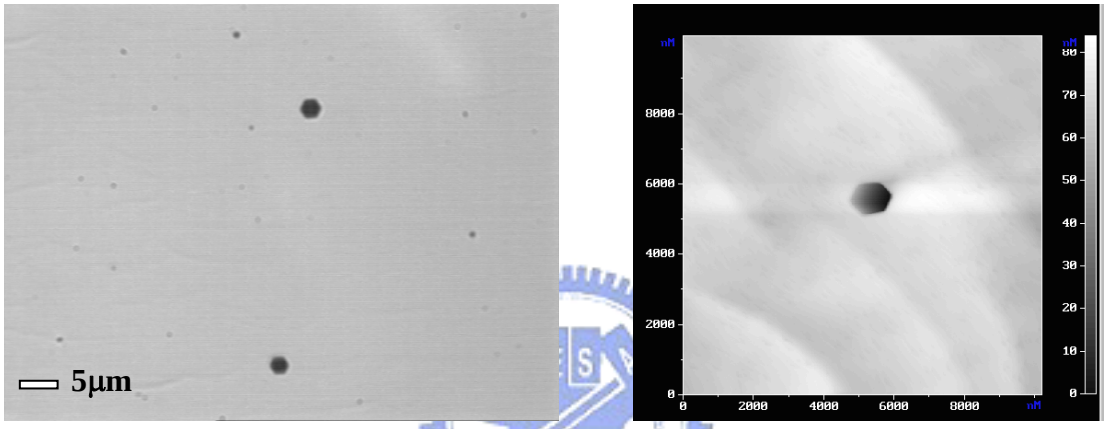

Sample B

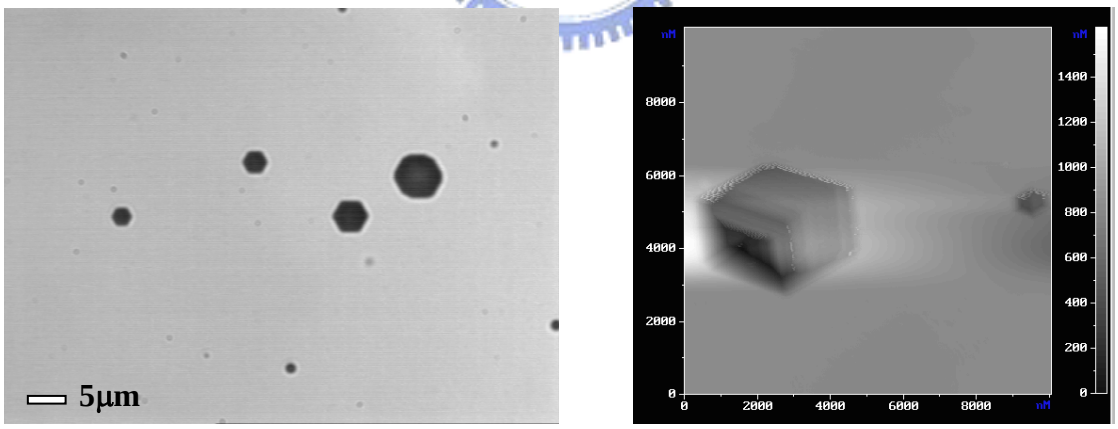

Sample C

Fig.4-1-1 Micrographs and AFM images (10μm x 10μm) of samples A, B, and C

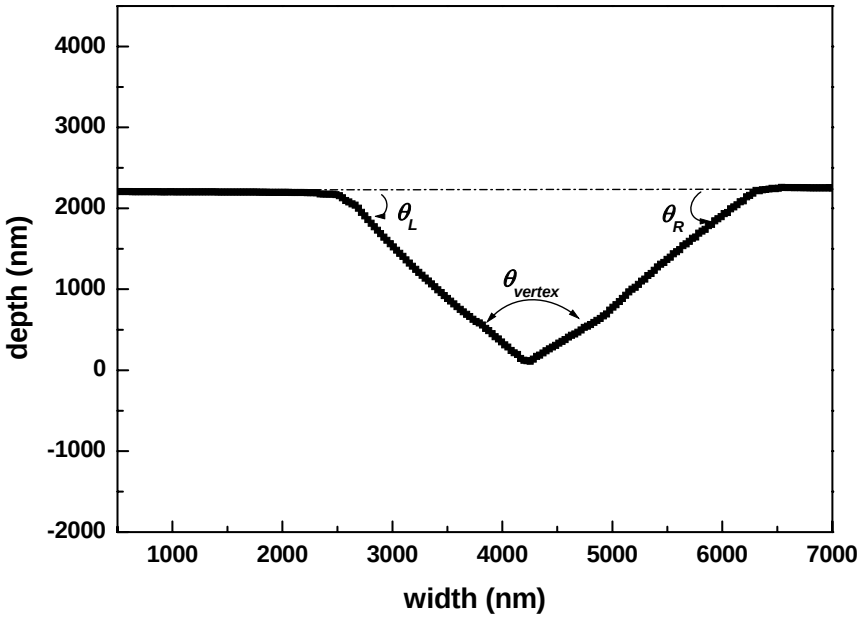

(a)

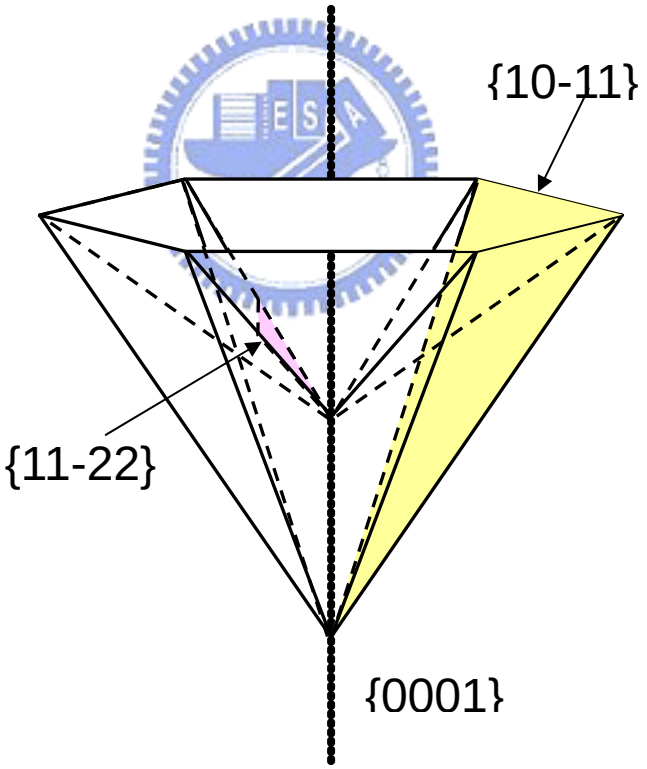

(b)

Fig.4-1-2 (a) Cross sectional view of V-defect and (b) the schematic illustration of a V-defect

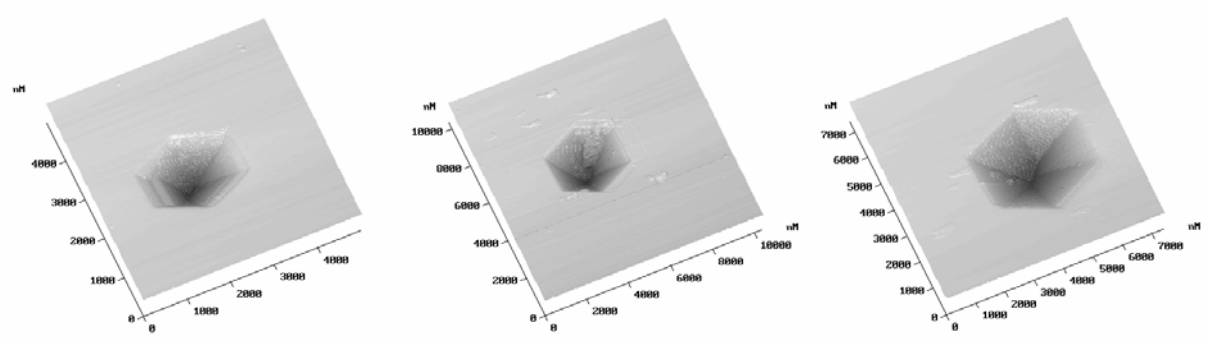

(a) 5μm x 5μm (b) 10μm x 10μm (c) 7μm x 7μm

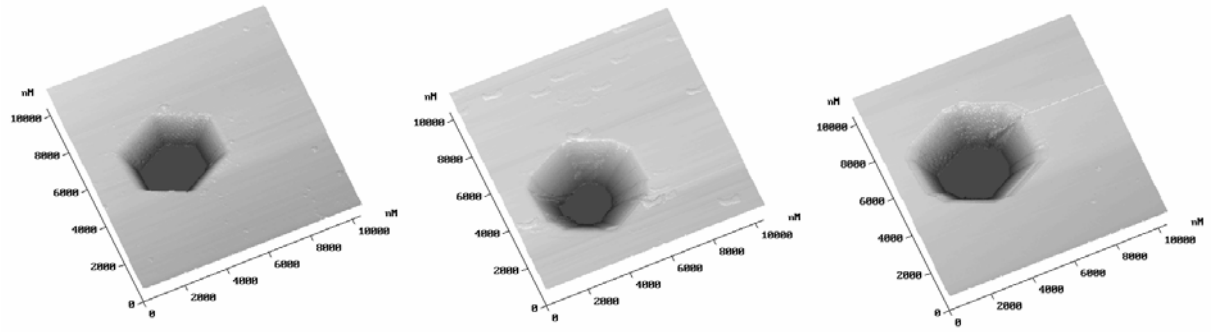

(d) 10μm x 10μm (e) 10μm x 10μm (f) 10μm x 10μm

Fig.4-1-3 3D AFM images of V-defects with diameter: (a) 1.9μm (b) 3.2μm (c) 4.0μm (d) 4.8μm (e) 5.2μm (f) 5.9μm on sample C.

angles	1.9μm	3.2μm	4.0μm	4.8μm	5.2μm	5.9μm
left angle (°)	48.7	50.4	51.7	52.2	54.2	51.9
right angle (°)	50.3	51.7	46.0	52.2	48.4	46.1
vertex angle (°)	81.0	77.9	82.3	75.6	77.4	82.0

Table 4-1-1 Vertex angle in V-defects of different size

4.2 Raman Spectra of V-defects of Different Doping Concentrations

To investigate the influence of doping concentration on Raman scattering of V-defects, we show typical back-scattering μ-Raman spectra of different doping concentrations (A, B, and C) and of *u*-GaN and *n*-GaN. As shown in Fig.4-2-1, we present the μ-Raman spectra on the plain region of each sample, the peak at ~568cm^{-1} corresponds to the E_2 phonon mode of GaN wurtzite structure, and the feature ranged from 730cm^{-1} to 750 cm^{-1} is the A_1(LO) related vibration mode. It is clear that in the *u*-GaN and *n*-GaN samples, the A_1(LO) related phonon mode appears like one Lorentzian peak only. However in samples A, B, and C, the A_1(LO) related mode is obviously consisted of two peaks. Peak positions are plotted in Fig.4-2-2 with the x-axis for the doping concentration obtained from Hall measurements. The dashed lines across the figure mark the E_2 and A_1(LO) positions of *u*-GaN. Peaks at ~568cm^{-1} and 734cm^{-1} are the E_2 and A_1(LO) of GaN from previous studies[8,12]. The spectral feature larger than 739cm^{-1} in samples A, B, C, and *n*-GaN are attributed to the coupling effect of LO phonon and plasmon caused by noticeable doping concentration as discussed in other studies[8,13,14]. Thus, we are confident that two LO related peaks in samples A, B, and C are from two GaN layers, respectively. The A_1(LO) at 734cm^{-1} comes from *u*-GaN layer while the LO phonon-plasmon coupling (LOPC) larger than 739cm^{-1} comes from *n*-GaN layer.

In contrast, Raman spectra of 3.3 μm V-defect on samples A, B, and C are

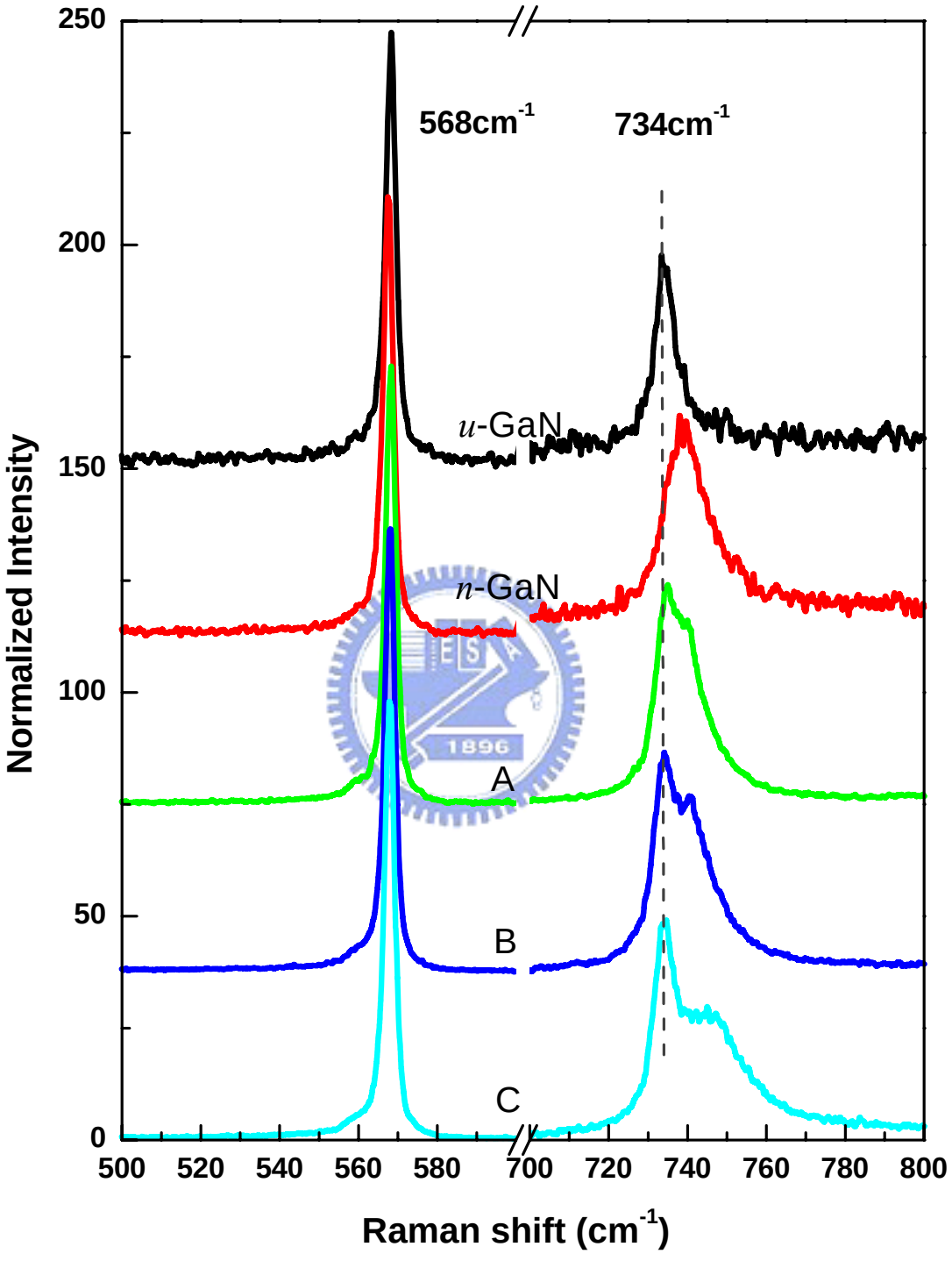

Fig.4-2-1 Raman spectra of plain region in each sample

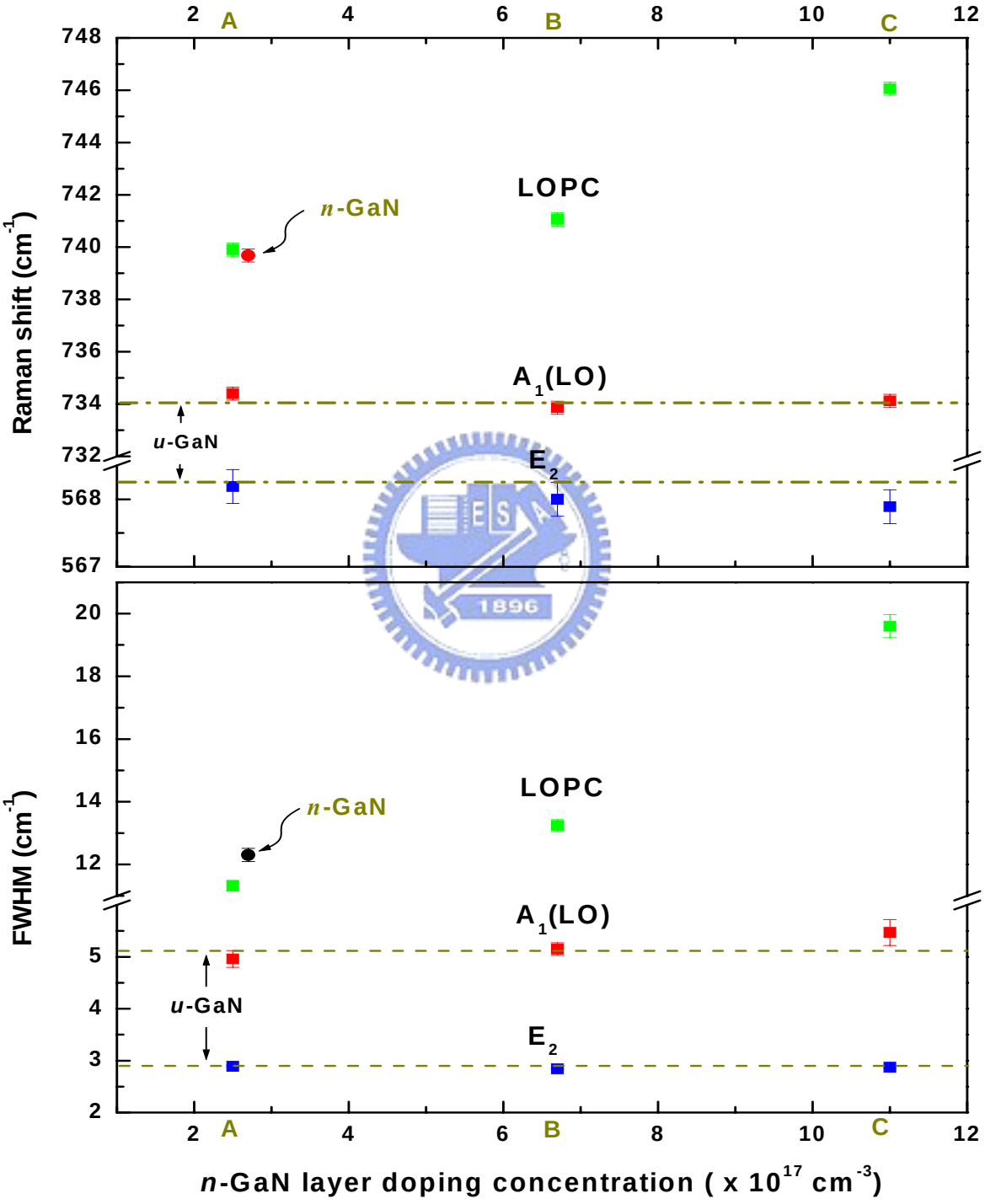

Fig.4-2-2 Phonon modes on plain region of different doping concentrations

shown in Fig.4-2-3. For comparison, we also show the spectra from the plain region. It is clear that spectra inside V-defects are not only broadened but also have larger shifts. The peak position and full width at half maxima (FWHM) are plotted in Fig.4-2-4. The overall variation of LO related vibration modes with the increasing doping concentration inside V-defects is similar to that on the plain region, as shown in Fig.4-2-5. However, noticeable blue shift as large as 3.4cm^{-1} and increased broadening by 4.9cm^{-1} of LO related peaks between plain and V-defects are observed. This phenomenon is believed to be due to high carrier density inside V-defects. Such a blue-shift will be discussed in the next section by varying V-defect size.

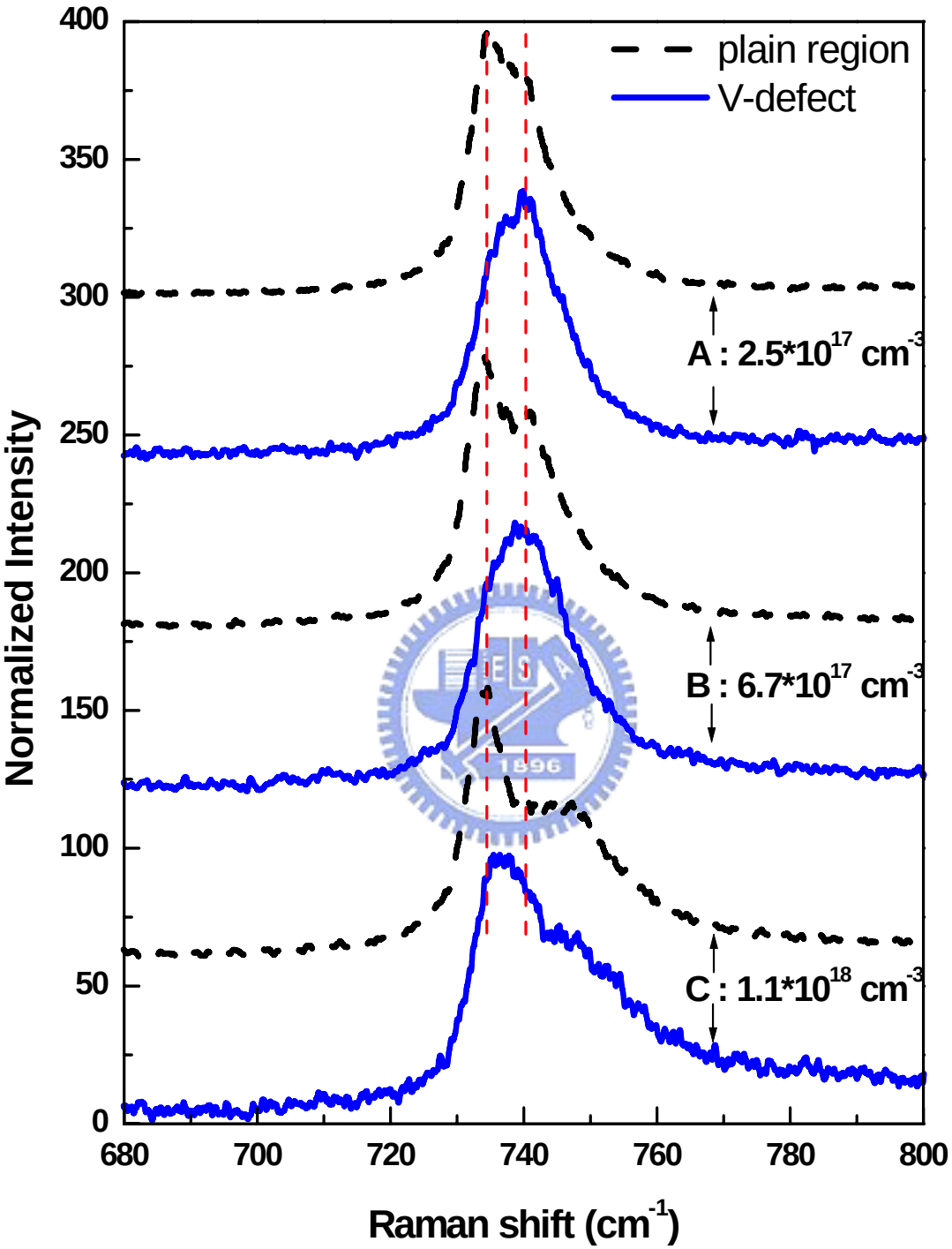

Fig.4-2-3 LO related modes in plain (dashed lines) and 3.3μm V-defects (solid lines) of sample A, B, and C

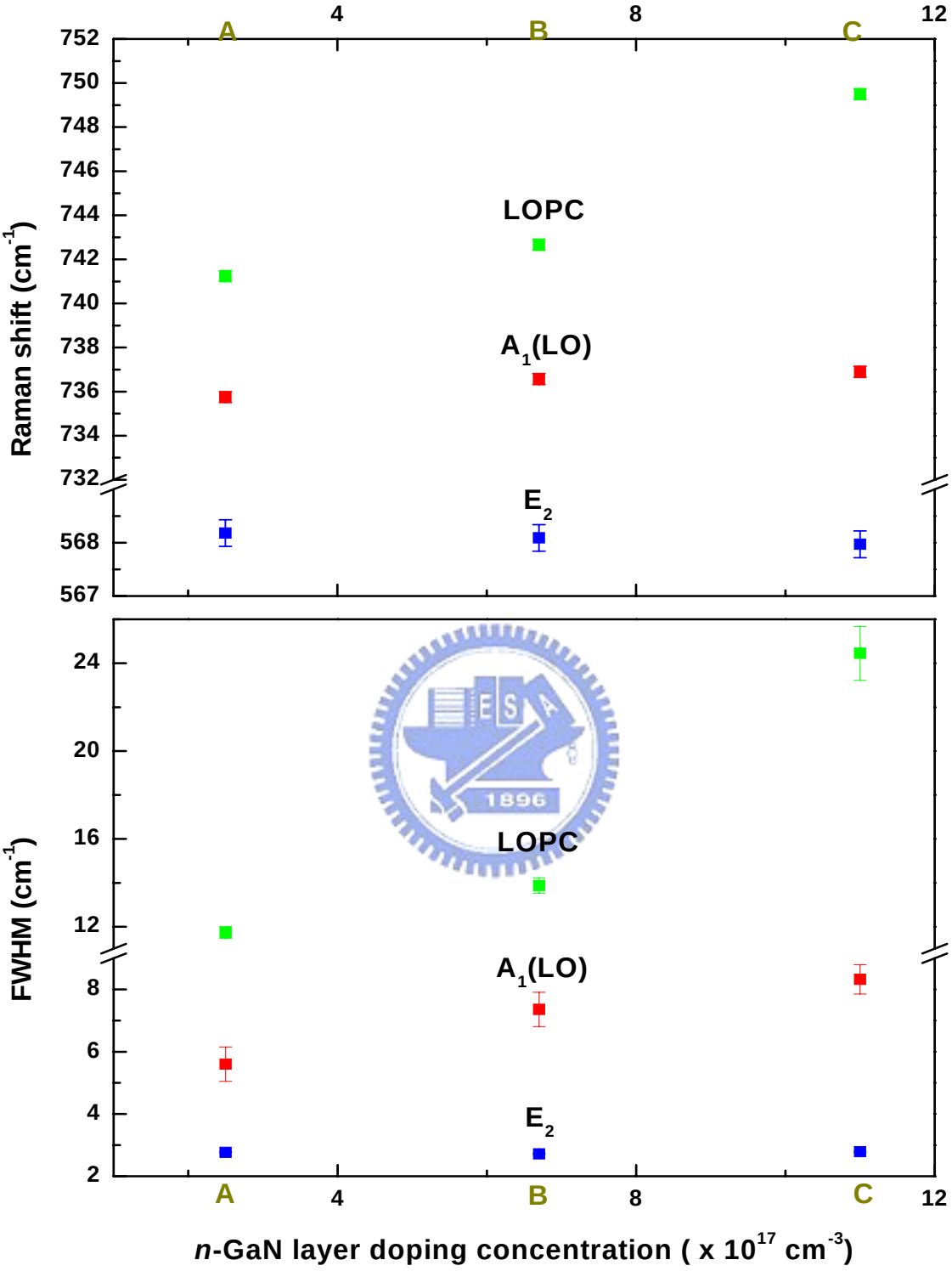

Fig.4-2-4 Phonon modes on 3.3 μm V-defects of different doping concentration

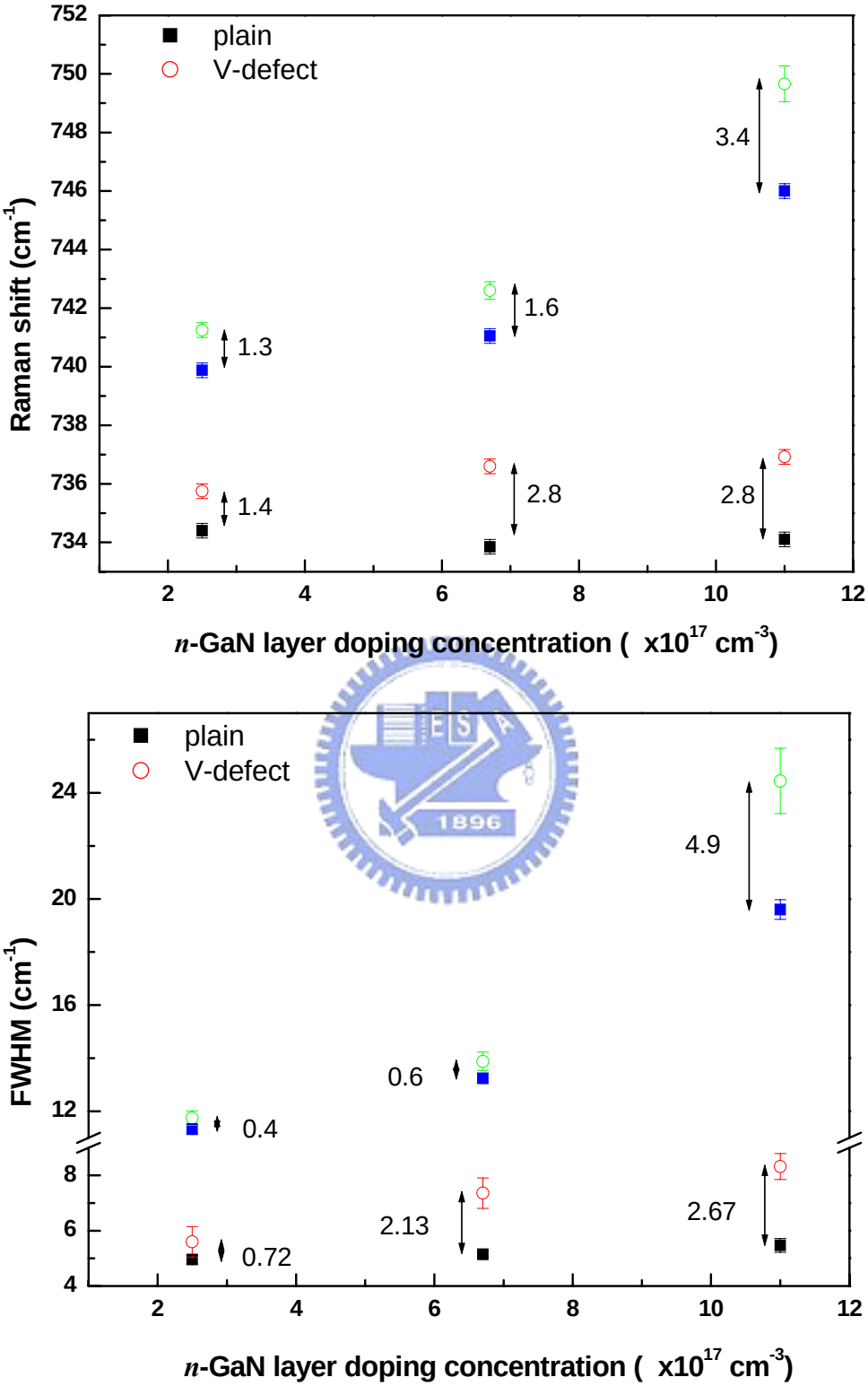

Fig.4-2-5 (a) peak positions and (b) FWHM of difference between plain region and V-defects in different doping concentration

4-3 Raman Spectra of V-defects of Different Size

To investigate the influence of V-defect size on Raman modes distribution, we measured the μ-Raman spectra from different V-defects in the range of 2.7μm~6.0μm on sample C. All spectra were acquired at room temperature, and the spectral resolution is about 0.5cm^{-1}. Shown in Fig.4-3-1 are microscopic images and Raman spectra of these V-defects, which are normalized to the E_2 mode intensity. On the plain region, Raman modes at 567.3cm^{-1}, 734.0cm^{-1}, and 746.3cm^{-1} correspond to E_2, A_1(LO) of *u*-GaN layer, and LOPC of *n*-GaN layer. Forbidden E_1(TO) mode appeared at 558.5cm^{-1} on the plain is believed to be caused by misorientations or defects[15,16]. As the V-defect size increases, forbidden A_1(TO) (531.4cm^{-1}) and E_1(TO) (558.5cm^{-1}) modes become more distinct and LO related modes show larger blue-shift, although the E_2 mode remains unshifted. While the A_1(LO) intensity of *u*-GaN layer shows insignificant change, the LOPC intensity from *n*-GaN becomes feeble with the increasing of V-defect size, because of the reduction of effective scattering volume in *n*-GaN layer.

According to the selection rule, A_1(TO) and E_1(TO) appearing in x(,)x scattering geometry are forbidden in the back-scattering geometry z(,)z[8,12]. In our study, E_1(TO) signal is weak in small V-defects and increases with the increasing size, while A_1(TO) is hardly observed until V-defect size is larger than 4.5μm. Since the behavior of V-defect is similar to the ELO structure, we also suggest that the appearance of forbidden A_1(TO) and E_1(TO) modes may be

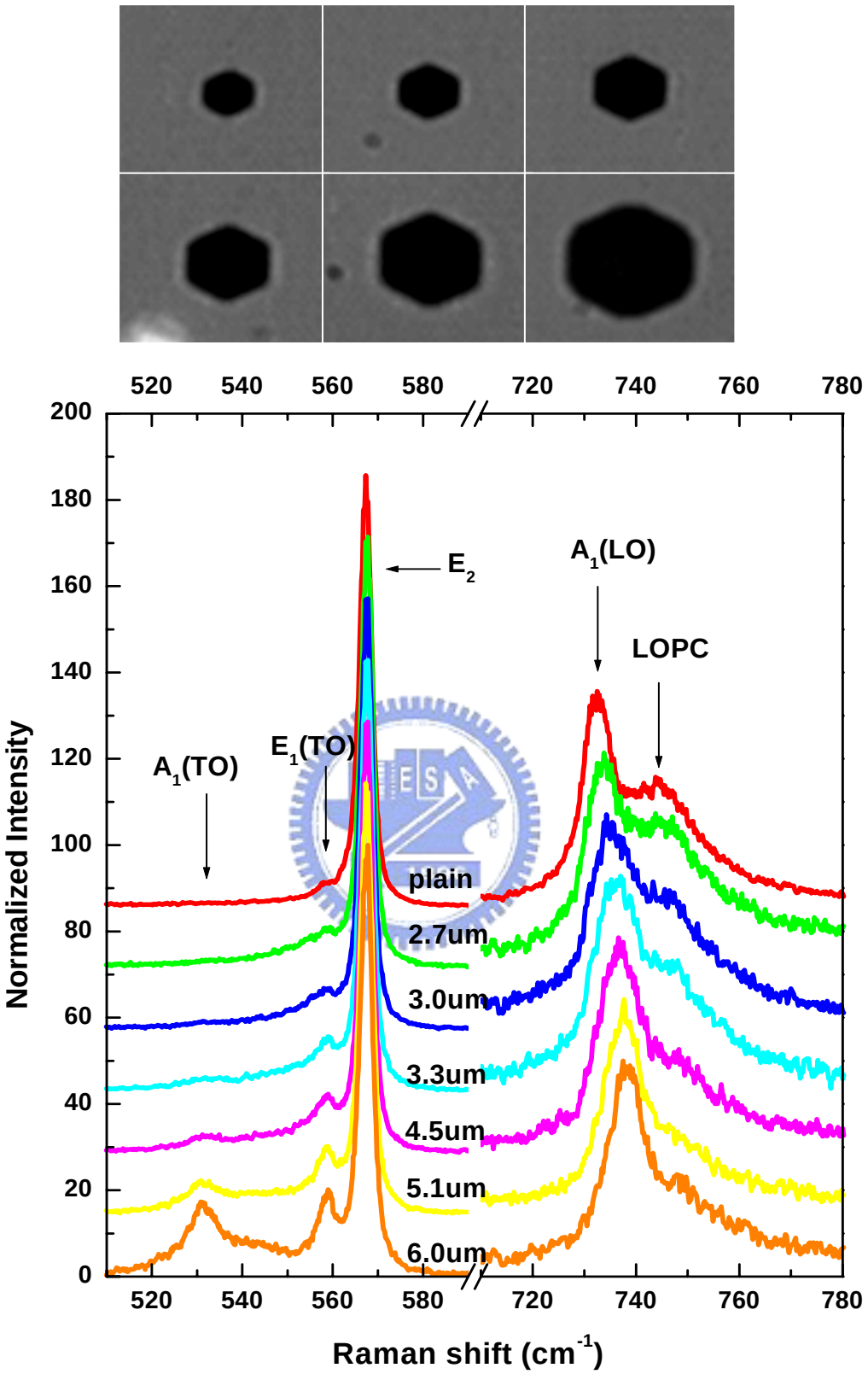

Fig.4-3-1 Optical micrographs of V-defects in sample C from top left to bottom right: 2.7、3.0、3.3、4.5、5.1 and 6.0μm and their Raman spectra

caused by the right angle scattering, because of the change of the landform, as that suggested by Hao[7] for the ELO pyramid structure. The distinct signal intensity of forbidden modes in larger V-defects is thus attributed to higher defect and dislocation density inside them.

Three phonon modes, E_2, A_1(LO) of *u*-GaN layer, and LOPC of *n*-GaN layer are fitted using Lorentzian peaks. Fig.4-3-2 shows the Raman shifts for each V-defect size. The dashed lines across the figure mark the three phonon frequencies of the plain region. Notable displacements of A_1(LO) and LOPC can be observed between plain region and inside V-defect, while no evident change for the E_2 mode. The blue-shift differences of A_1(LO) and LOPC increase from 1.2 to 5.6cm^{-1} and 1.5 to 5.8 cm^{-1},respectively, as V-defect size increases from 2.7μm to 6.0μm. The blue-shift may be due to the following reasons： (1) quasi-LO effect caused by the morphology. (2) V-defect experiences a compressive strain. (3) LO phonon-plasmon coupling caused by large carrier concentration.

According to previous studies[17,18], the quasi-LO yields by mixing A_1 and E_1 modes for an intermediate propagation direction between parallel and perpendicular to the crystal axis. The intermediate frequency ω_Q is then described as a combination of A_1(LO) and E_1(LO) with an included angle θ between the propagation direction and the c-axis：

$$\omega^2_Q(\mathrm{LO}) = \omega^2(\mathrm{A_1[LO]})\cos^2\theta + \omega^2(\mathrm{E_1[LO]})\sin^2\theta.$$

The frequencies of A_1(LO) in *u*-GaN layer suggest that bottom angles of

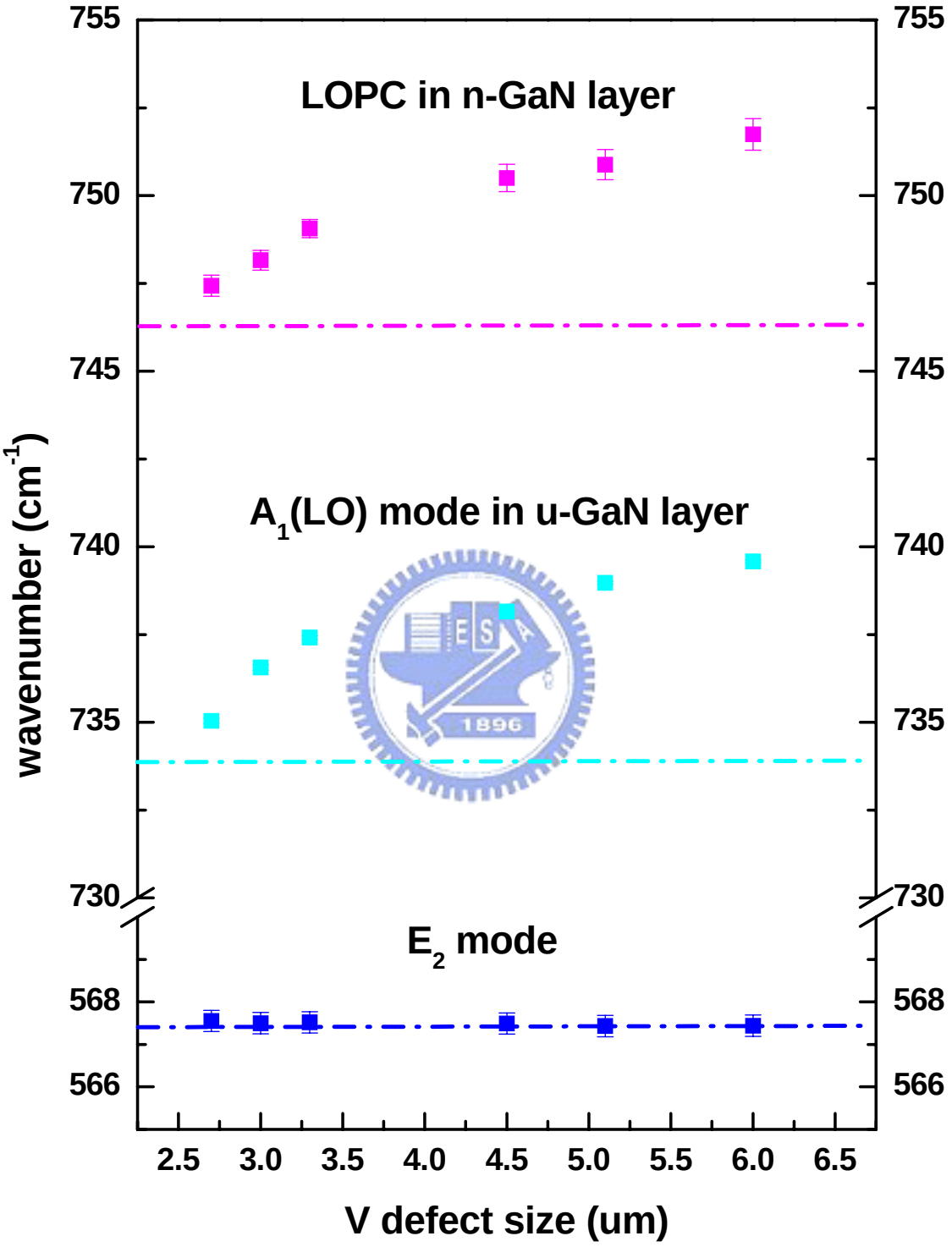

Fig.4-3-2 E_2, A_1(LO), and LOPC phonon modes in V-defects of different size

V-defects should vary from 133° to 53°, corresponding to the variation of included angle θ from 23.5° to 63.5°, as the size increases from 2.7μm to 6.0μm if the quasi-LO effect is the major cause of displacements. However, the morphology profiles from AFM show that no such huge variation appears in bottom angles of V-defects. Thus, we believe that the quasi-LO effect is not the major cause for the blue-shift.

Next, the strain relaxation in V-defect is considered, since Raman spectra are also sensitive to the strain inside lattice. In the Demangeot *et al*'s study, they evaluated the stress-shift rate as 0.8cm^{-1}/GPa for the A_1(LO) mode and 2.9cm^{-1}/GPa for the E_2 mode[19]. It implies that the E_2 mode is more sensitive than the A_1(LO) under stress. In our study, although the A_1(LO) is blue shifted by as much as 5.8cm^{-1} in a large V-defect as compared with the plain region, the E_2 mode remains almost at the same peak position and FWHM. We believe that the strain effect is not the main cause for the blue shift of LO related phonon mode either.

Another possibility of the distinct blue-shift is the LO phonon coupled with carriers gathering inside V-defects with dislocations lying beneath. Some experimental[20~23] and theoretical[24,25] works suggested that threading dislocations in *n*-type GaN can trap Ga vacancy (V_{Ga}) and Ga vacancy complexes with oxygen (V_{Ga}-O_N). They have acceptor-like nature due to unpaired dangling bonds, and are negatively charged. M. S. Jeong[3] attributed the yellow luminescence (YL) inside V-defects in InGaN/GaN multiple-quantum wells to

acceptor-like level contributed by Ga vacancy complexes. Motoki *et al*'s[11] studied cross-sectional TEM images of V-defects on as-grown GaN which indicate higher dislocation density below V-defects than that in plain region. Raman spectra in our study revealed the similar results as in the published papers. In samples A, B, and C, A_1(LO) of *u*-GaN layer and LOPC mode of *n*-GaN layer inside V-defects experienced stronger coupling than that in plain region as shown by the increased blue-shift and broadening in Fig.4-3-2. The coupling effect of the LO related peaks is associated with high electron density. Thus, as the V-defect size increases, the quantity of V_{Ga} on facets of V-defect and dislocations under it also increase.

For double checking the appearance of forbidden modes and LO related blue shift, line scan Raman spectra of 6.0μm V-defect are shown in Fig.4-3-3. Spectrum at position 1, which denotes the plain region next to V-defect, shows common positions of LO-related modes and no appearance of A_1(TO)、E_1(TO). As the 2μm laser spot moves gradually into V-defect center (position 4), forbidden A_1(TO)、E_1(TO) modes become significant and distinct blue shift of A_1(LO) in *u*-GaN layer is easily observed. Besides, the LOPC mode intensity is weakened in central V-defect, because of the decrease of effective scattering volume of *n*-GaN layer. Forbidden modes disappear again and LO-related peaks shift back as the incident laser spot moves out side the V-defect region (position 7). The A_1(LO) varies from 734 to 740 cm-1 gradually as the probe spot moves from plain region to the center of the V-defect. This indicates that a higher

electron density occurs in the center than that in the side walls of V-defect and plain region. However, forbidden modes A_1(TO) and E_1(TO) appear not only in the center but also the side walls of V-defect. It shows that the major reason of forbidden modes appearance is the right angle scattering because of the change of morphology, which breaks the selection rule due to high dislocation density underneath the surface.

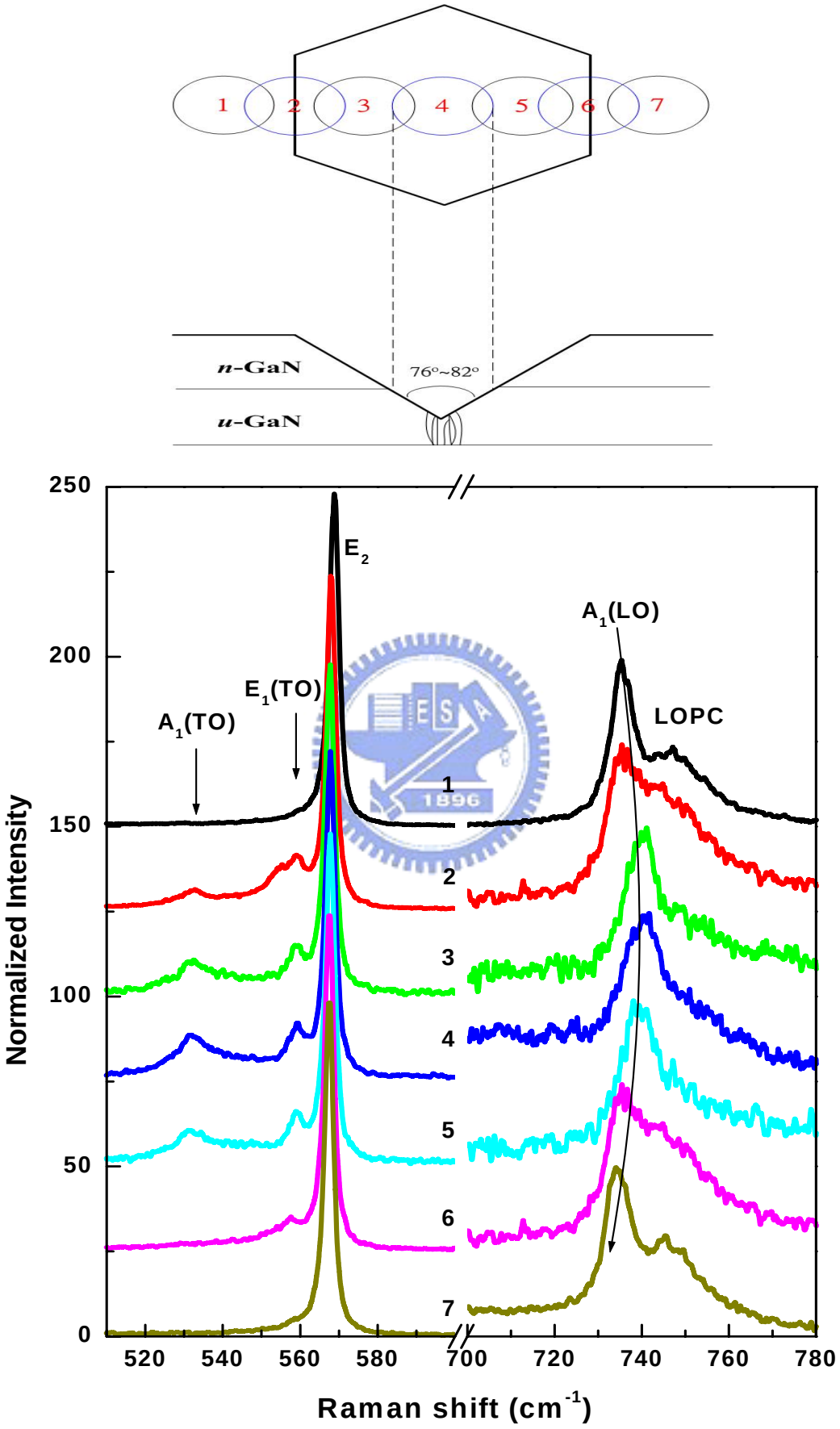

Fig.4-3-3 Line scan Raman spectra of 6.0μm V-defect

4-4 Simulation by LOPC Model

When plasmon damping is significant, LO phonon-plasmon coupling is displayed as a shift of the LO phonon mode[8,12]. The plasma frequency ω_p can be deduced by fitting the coupled A_1(LO) phonon-plasmon peak to the following expression as introduced in section2-3:

$$I_A = const \cdot A(\omega) \cdot \mathrm{Im}\{-\varepsilon(\omega)^{-1}\},$$

where $\varepsilon(\omega)$ is the dielectric function, and $A(\omega)$ is related to the deformation-potential and the electro-optic mechanism. $A(\omega)$ is in the form of

$$A(\omega) = 1 + 2C\frac{\omega_{TO}^2}{\delta}[\omega_p^2\gamma(\omega_{TO}^2 - \omega^2) - \omega^2\Gamma(\omega^2 + \gamma^2 - \omega_p^2)]$$
$$+ C^2\{\omega_p^2[\gamma(\omega_{LO}^2 - \omega_{TO}^2) + \Gamma(\omega_p^2 - 2\omega^2)] + \omega^2\Gamma(\omega^2 + \gamma^2)\} \times (\frac{\omega_{TO}^4}{\delta(\omega_{LO}^2 - \omega_{TO}^2)}),$$

where

$$\delta = \omega_p^2\gamma\{(\omega\Gamma)^2 + (\omega_{TO}^2 - \omega^2)^2\} + \omega^2\Gamma(\omega^2 + \gamma^2)(\omega_{LO}^2 - \omega_{TO}^2),$$

C is the Faust-Henry coefficient, ω_p is the plasma frequency, ω_{TO} and ω_{LO} are the TO and LO phonon frequencies, and Γ and γ are the phonon and plasmon damping constants, respectively. The dielectric function $\varepsilon(\omega)$ here is a combination of the contribution from phonons and plasmons:

$$\varepsilon(\omega) = \varepsilon_\infty(1 + \frac{\omega_{LO}^2 - \omega_{TO}^2}{\omega_{TO}^2 - \omega^2 - i\omega\Gamma} - \frac{\omega_p^2}{\omega(\omega + i\gamma)}).$$

The plasma frequency ω_p is given by,

$$\omega_p = \sqrt{\left(\frac{4\pi ne^2}{\varepsilon_\infty m^*}\right)},$$

where n is the free carrier concentration and m^* is the effective mass of the free

carriers. For fitting purpose, Faust-Henry coefficient C=0.4, ω_{TO}=531cm^{-1}, ω_{LO}=734cm^{-1}, m^*=0.2m_o, and ε_∞=5.35 for GaN were used[8,12].

As shown in Fig.4-4-1, experimental and theoretical line shape of LPP modes in 3.3μm V-defects and plain region on samples A, B, and C fit well to each other. The fitting results are summarized in Fig.4-4-2 and tabulated in Table4-4-1. An obvious concentration difference can be observed between plain and V-defect, especially in *u*-GaN layer. The free carrier concentrations increase from 5*10^{16}cm^{-3} in plain region to ~2*10^{17}cm^{-3} in V-defects for *u*-GaN by 4 times, while free carrier concentration increases in *n*-GaN layer is only a fraction. The large carrier density difference between plain region and V-defects indicate that additional carriers are provided by V-defects because of higher dislocation density lying beneath. The difference of electron concentration between that obtained from Hall measurements and Raman spectra had been discussed in other studies by Go¨tz, Xu, and Florescu [26~28]. They suggest that n_R<n_H is a result of the fact that the latter contains contributions from both the epilayer and narrow GaN/sapphire interfacial region, while the former is primarily from the epilayer.

Raman spectra of V-defects of different size discussed in section 4-3 are simulated using the LOPC model as shown in Fig.4-4-3. The fitting results are summarized in Fig.4-4-4. Dashed lines across the figure denote n_H and n_R in the plain region, respectively. Since the carrier concentration in *u*-GaN layer of 2.7μm V-defect is so low, the LOPC effect is nearly degenerate with the LO

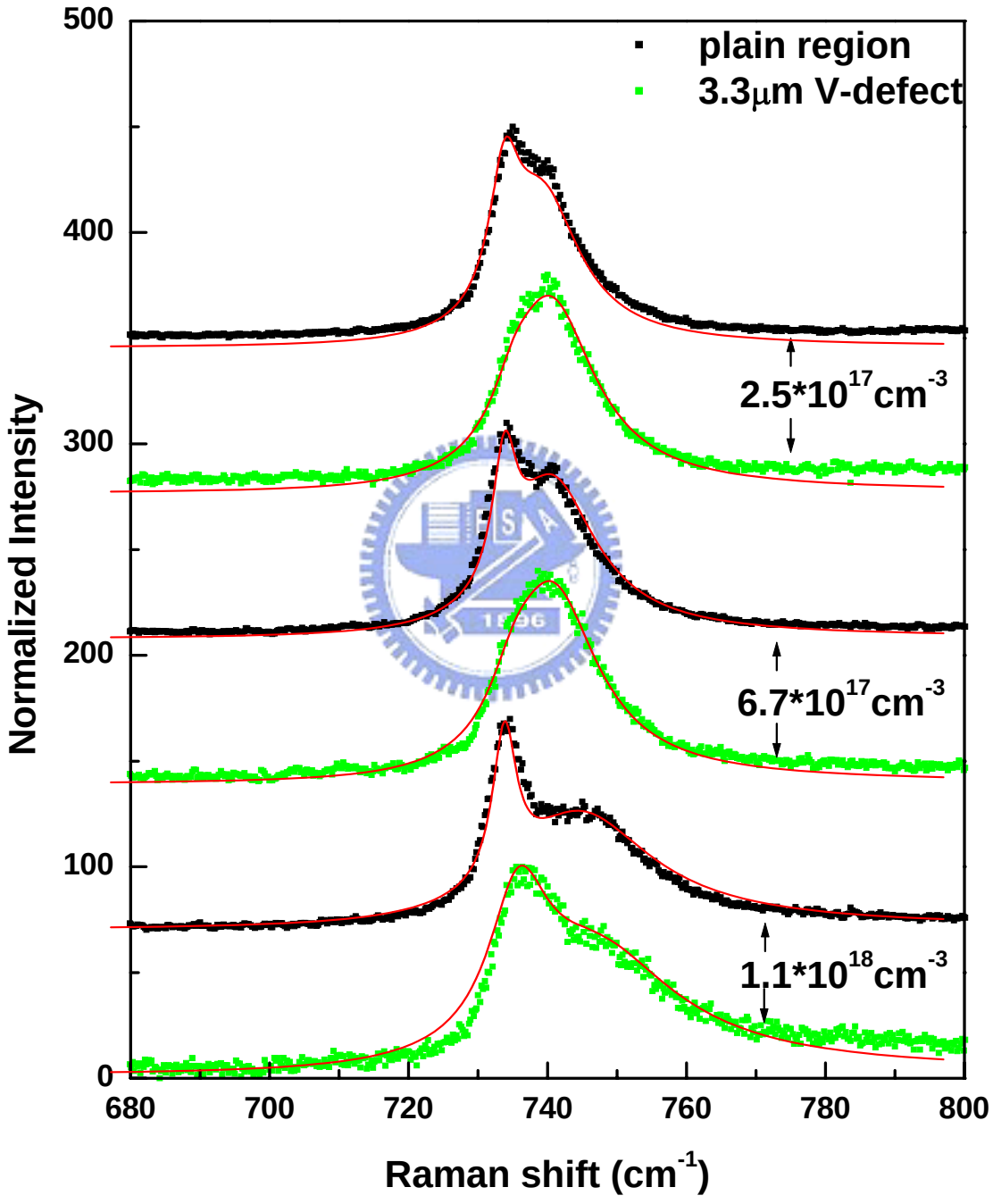

Fig.4-4-1 experiential and theoretical line shape in samples A, B, and C

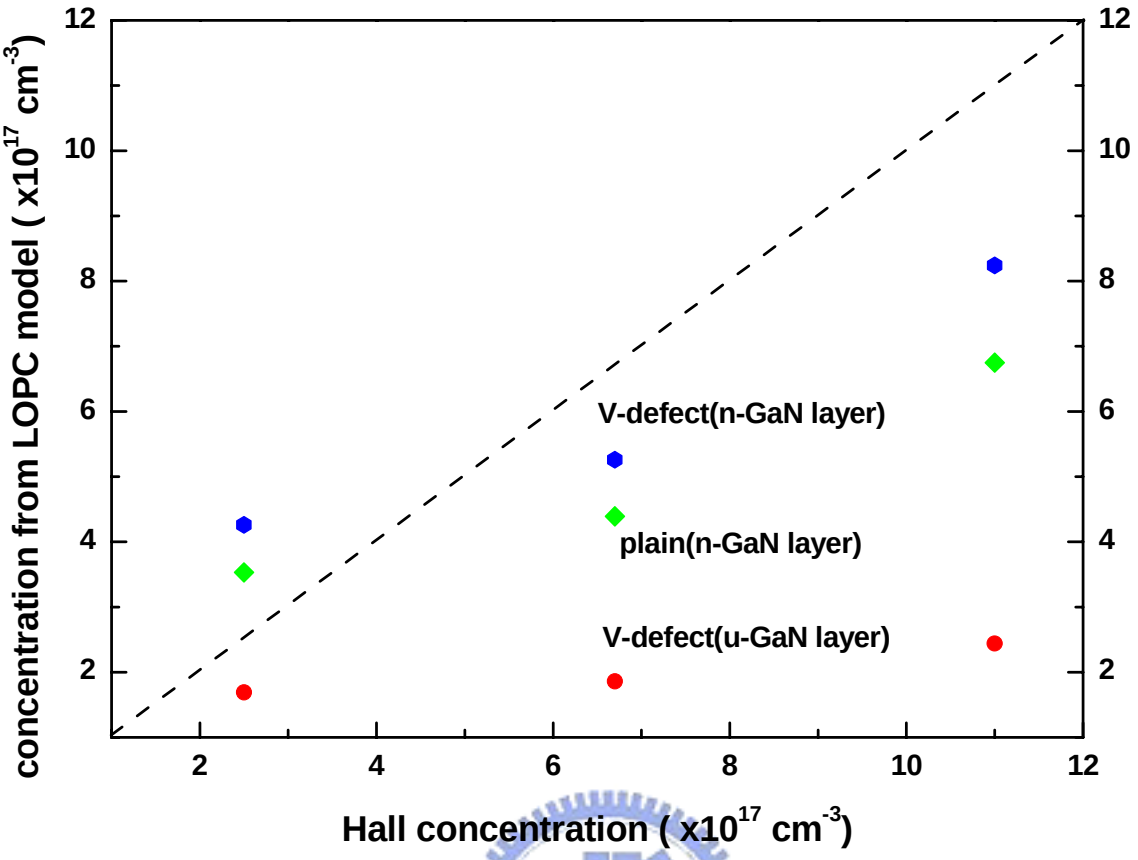

Fig.4-4-2 Comparison between n_H and n_R

	A(n_H=2.5*10^{17}cm^{-3})		B (n_H=6.7*10^{17}cm^{-3})		C (n_H=1.1*10^{18}cm^{-3})	
	ω_p(cm^{-1})	n_e(cm^{-3})	ω_p(cm^{-1})	n_e(10^{17}cm^{-3})	ω_p(cm^{-1})	n_e(10^{17}cm^{-3})
plain(*u*-GaN)	--	--	--	--	--	--
V-defect(*u*-GaN)	119	1.7*10^{17}	125	1.9*10^{17}	143	2.4*10^{17}
plain(*n* -GaN)	172	3.5*10^{17}	192	4.4*10^{17}	238	6.7*10^{17}
V-defect(*n*-GaN)	189	4.2*10^{17}	210	5.3*10^{17}	263	8.2*10^{17}

Table4-4-1 Fitting results of the LOPC effect

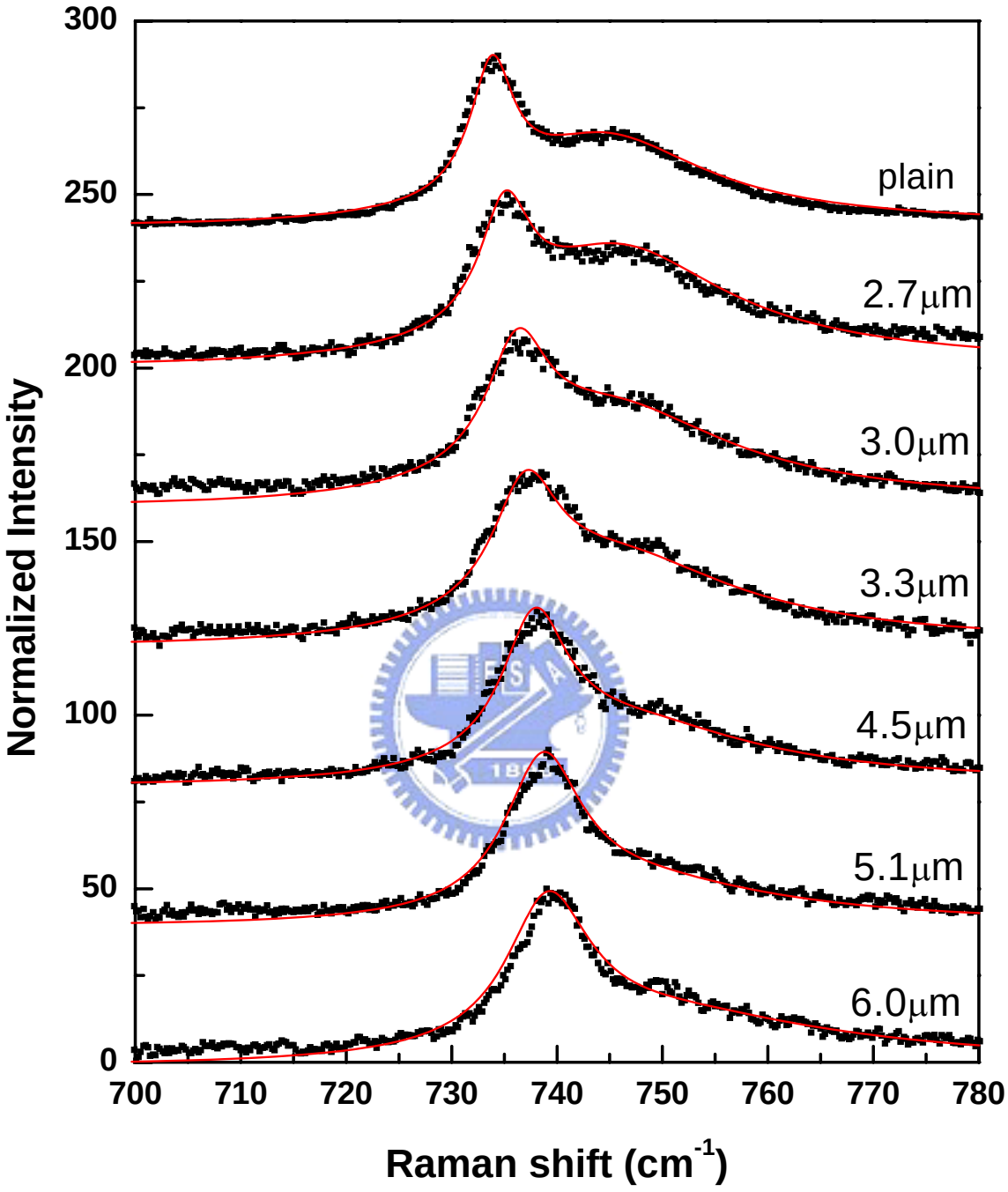

Fig.4-4-3 Experiential and theoretical line shapes of different size V-defects

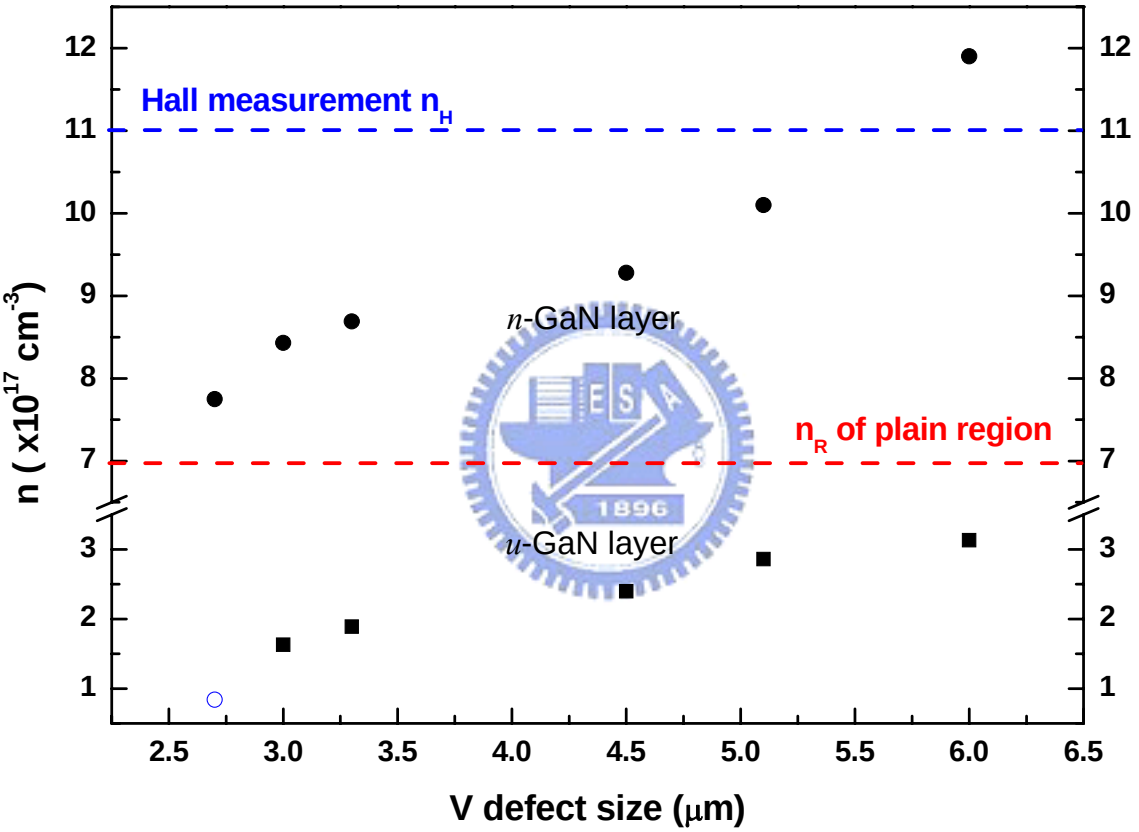

Fig.4-4-4 Free electron concentration calculated in different size V-defect

peak, the uncertain concentration is indicated as the hollow circle. Free carrier concentrations inside V-defects increase with the defect size. This suggests higher dislocation density inside larger V-defects that provides more free carriers.

As the dislocation density is taken into consideration, the effective electron density n_e can be written as $n_e = n_d + N_A^- + N_{dis} \cdot (f / c)$, where n_d is the volume doping density, N_A^- is the corresponding unintentional acceptor and is ignorable in our samples, and f is the filling factor described as $f=c/l$, where c is the lattice spacing along GaN (0001) direction and l is the spacing between occupied sites. The filling factor f is in the range of 0.7~0.8 for the free carrier concentration of $5*10^{16}cm^{-3}$ [29].Thus, the effective electron density of *u*-GaN layer inside 3.0μm and 6.0μm V-defects can be calculated by using f=0.75.

$$1.7\times10^{17}(cm^{-3}) = 5\times10^{16}(cm^{-3}) + \frac{0.75}{5.18\times10^{-8}(cm)} \times N_{dis\ 3\mu m}(cm^{-2})$$

$$3.1\times10^{17}(cm^{-3}) = 5\times10^{16}(cm^{-3}) + \frac{0.75}{5.18\times10^{-8}(cm)} \times N_{dis\ 6\mu m}(cm^{-2})$$

It suggests that the localized dislocation density inside 3.0 and 6.0μm V-defects is 0.9 and $1.8*10^{10}cm^{-2}$, respectively. The carriers provided by V-defect become majority and increase *n* for *u*-GaN layer. As mentioned in other studies, dislocation density ranged from 10^8cm^{-2} to 10^9cm^{-2} in GaN films and hardly increases *n*. High dislocation density ($\geqq 10^{10}cm^{-2}$) inside V-defects sounds reasonable as indicated in Motoki's[11] report although no studies have mentioned about the order of dislocation density inside V-defects. Combining the results of

the LOPC model and the calculation from effective charge density, we suggest that the dislocation density inside V-defect is 10 times larger than that in plain region.